Second harmonic generation in AlGaAs photonic wires using low power continuous wave light

D. Duchesne,[1,*] K. A. Rutkowska,[1,2] M. Volatier,[7] F. Légaré,[1] S. Delprat,[1] M. Chaker,[1] D. Modotto,[3] A. Locatelli,[3] C. De Angelis,[3] M. Sorel,[4] D. N. Christodoulides,[5] G. Salamo,[6] R. Arès,[7] V. Aimez,[7] and R. Morandotti[1]

[1]INRS-EMT, 1650 Boulevard Lionel Boulet, Varennes, Québec, J3X 1S2, Canada
[2]Faculty of Physics, Warsaw University of Technology, Warsaw, PL-00662, Poland
[3]Dipartimento di Ingegneria dell'Informazione, Università di Brescia, via Branze 38, Brescia, 25123, Italy
[4]Department of Electrical and Electronic Engineering, University of Glasgow, Glasgow, G12 8QQ, Scotland
[5]College of Optics & Photonics-CREOL & FPCE, University of Central Florida, Orlando, Florida, 32816, USA
[6]Dept. of Physics, University of Arkansas, Fayetteville, Arkansas, 72701, USA
[7]Centre de Recherche en Nanofabrication et en Nanocaractérisation (CRN²), Université de Sherbrooke, Sherbrooke, Québec, J1K 2R1, Canada
**david.duchesne@emt.inrs.ca*

Abstract: We report modal phase matched (MPM) second harmonic generation (SHG) in high-index contrast AlGaAs sub-micron ridge waveguides, by way of sub-mW continuous wave powers at telecommunication wavelengths. We achieve an experimental normalized conversion efficiency of ~14%/W/cm^2, obtained through a careful sub-wavelength design supporting both the phase matching requirement and a significant overlap efficiency. Furthermore, the weak anomalous dispersion, robust fabrication technology and possible geometrical and thermal tuning of the device functionality enable a fully integrated multi-functional chip for several critical areas in telecommunications, including wavelength (time) division multiplexing and quantum entanglement.

OCIS codes: (190.2620) Harmonic generation and mixing; (130.3120) Integrated optics devices; (130.7405) Wavelength conversion devices; (230.7370) Waveguides; (160.6000) Semiconductor materials.

References and links

1. M. M. Fejer, "Nonlinear optical frequency conversion," Phys. Today **47**(5), 25–32 (1994).
2. A. Arie, K. Fradkin-Kashi, and Y. Shreberk, "Frequency conversion in novel materials and its application to high resolution gas sensing," Opt. Lasers Eng. **37**(2-3), 159–170 (2002).
3. W. Petrich, "Mid-infrared and Raman spectroscopy for medical diagnostics," Appl. Spectrosc. Rev. **36**(2&3), 181–237 (2001).
4. R. F. Curl and F. K. Tittel, "Tunable infrared laser spectroscopy," Annu. Rep. Prog. Chem. C **98**, 217–270 (2002).
5. S. Tanzilli, H. De Riedmatten, W. Tittel, H. Zbinden, P. Baldi, M. De Micheli, D. B. Ostrowsky, and N. Gisin, "Highly efficient photon-pair source using periodically poled lithium niobate waveguide," Electron. Lett. **37**(1), 26–28 (2001).
6. C. Langrock, S. Kumar, J. E. McGeehan, A. E. Willner, and M. M. Fejer, "All-optical signal processing using $\chi(2)$ nonlinearities in guided wave devices," J. Lightwave Technol. **24**(7), 2579–2592 (2006).
7. A. M. Zheltikov, "Limiting efficiencies of second-harmonic generation and cascaded $\chi(2)$ processes in quadratically nonlinear photonic nanowires," Opt. Commun. **270**(2), 402–406 (2007).
8. R. W. Boyd, *Nonlinear Optics* Third Edition, (Academic Press, New York 2008).
9. A. Fiore, V. Berger, E. Rosencher, P. Bravetti, and J. Nagle, "Phase matching using an isotropic nonlinear optical material," Nature **391**(6666), 463–466 (1998).
10. T. C. Kowalczyk, K. D. Singer, and P. A. Cahill, "Anomalous-dispersion phase-matched second-harmonic generation in a polymer waveguide," Opt. Lett. **20**(22), 2273–2275 (1995).
11. K. R. Parameswaran, R. K. Route, J. R. Kurz, R. V. Roussev, M. M. Fejer, and M. Fujimura, "Highly efficient second-harmonic generation in buried waveguides formed by annealed and reverse proton exchange in periodically poled lithium niobate," Opt. Lett. **27**(3), 179–181 (2002).

#146909 - $15.00 USD Received 3 May 2011; revised 4 Jun 2011; accepted 7 Jun 2011; published 10 Jun 2011

12. W. Sohler and H. Suche, "Second-harmonic generation in Ti-diffused $LiNbO_3$ optical waveguides with 25% conversion efficiency," Appl. Phys. Lett. **33**(6), 518–520 (1978).
13. D. B. Anderson and J. T. Boyd, "Wideband CO_2 laser second harmonic generation phase matched in GaAs thin-film waveguides," Appl. Phys. Lett. **19**(8), 266–268 (1971).
14. S. Ducci, L. Lanco, V. Berger, A. De Rossi, V. Ortiz, and M. Calligaro, "Continuous-wave second-harmonic generation in modal phase matched semiconductor waveguides," Appl. Phys. Lett. **84**(16), 2974–2976 (2004).
15. S. V. Rao, K. Moutzouris, and M. Ebrahimzadeh, "Nonlinear frequency conversion in semiconductor optical waveguides using birefringent, modal and quasi-phase-matching techniques," J. Opt. A, Pure Appl. Opt. **6**(6), 569–584 (2004).
16. Y. Ishigame, T. Suhara, and H. Nishihara, "LiNbO(3) waveguide second-harmonic-generation device phase matched with a fan-out domain-inverted grating," Opt. Lett. **16**(6), 375–377 (1991).
17. X. Yu, L. Scaccabarozzi, J. S. Harris Jr, P. S. Kuo, and M. M. Fejer, "Efficient continuous wave second harmonic generation pumped at 1.55 μm in quasi-phasematched AlGaAs waveguides," Opt. Express **13**, 10742–10748 (2005).
18. A. Fiore, S. Janz, L. Delobel, P. van der Meer, P. Bravetti, V. Berger, E. Rosencher, and J. Nagle, "Second-harmonic generation at $\lambda = 1.6$ μm in $AlGaAs/Al_2O_3$ waveguides using birefringence phase matching," Appl. Phys. Lett. **72**(23), 2942–2944 (1998).
19. L. Scaccabarozzi, M. M. Fejer, Y. Huo, S. Fan, X. Yu, and J. S. Harris, "Enhanced second-harmonic generation in AlGaAs/AlxOy tightly confining waveguides and resonant cavities," Opt. Lett. **31**(24), 3626–3628 (2006).
20. A. Fiore, V. Berger, E. Rosencher, N. Laurent, S. Theilmann, N. Vodjdani, and J. Nagle, "Huge birefringence in selectively oxidized GaAs/AlAs optical waveguides," Appl. Phys. Lett. **68**(10), 1320–1322 (1996).
21. M. M. Fejer, G. A. Magel, D. H. Jundt, and R. L. Byer, "Quasi-phase-matched second harmonic generation: tuning and tolerances," IEEE J. Quantum Electron. **28**(11), 2631–2654 (1992).
22. P. Abolghasem, J. Han, B. J. Bijlani, A. Arjmand, and A. S. Helmy, "Highly efficient second-harmonic generation in monolithic matching layer enhanced AlxGa1-xAs Bragg reflection waveguides," IEEE Photon. Technol. Lett. **21**(19), 1462–1464 (2009).
23. Z. Yang, P. Chak, A. D. Bristow, H. M. van Driel, R. Iyer, J. S. Aitchison, A. L. Smirl, and J. E. Sipe, "Enhanced second-harmonic generation in AlGaAs microring resonators," Opt. Lett. **32**(7), 826–828 (2007).
24. P. Dong, J. Upham, A. Jugessur, and A. G. Kirk, "Observation of continuous-wave second-harmonic generation in semiconductor waveguide directional couplers," Opt. Express **14**(6), 2256–2262 (2006).
25. G. A. Siviloglou, S. Suntsov, R. El-Ganainy, R. Iwanow, G. I. Stegeman, D. N. Christodoulides, R. Morandotti, D. Modotto, A. Locatelli, C. De Angelis, F. Pozzi, C. R. Stanley, and M. Sorel, "Enhanced third-order nonlinear effects in optical AlGaAs nanowires," Opt. Express **14**(20), 9377–9384 (2006).
26. D. Duchesne, R. Morandotti, G. Siviloglou, R. El-Ganainy, G. Stegeman, D. Christodoulides, D. Modotto, A. Locatelli, C. De Angelis, F. Pozzi, and M. Sorel, "Nonlinear photonics in AlGaAs photonics nanowires: self phase and cross phase modulation," in *International Symposium on Signals, Systems and Electronics*, 475–478 (2007).
27. J. Meier, W. S. Mohammed, A. Jugessur, L. Qian, M. Mojahedi, and J. S. Aitchison, "Group velocity inversion in AlGaAs nanowires," Opt. Express **15**(20), 12755–12762 (2007).
28. V. Van, T. A. Ibrahim, K. Ritter, P. P. Absil, F. G. Johnson, R. Grove, J. Goldhar, and P. T. Ho, "All-optical nonlinear switching in GaAs-AlGaAs microring resonators," IEEE Photon. Technol. Lett. **14**(1), 74–76 (2002).
29. M. Bhashi, T. Kondo, R. Ito, S. Fukatsu, Y. Shiraki, K. Kumata, and S. S. Kano, "Determination of quadratic nonlinear optical coefficient of AlxGa1-xAs system by the method of reflected second harmonics," J. Appl. Phys. **74**(1), 596–601 (1993).
30. M. Volatier, D. Duchesne, R. Morandotti, R. Arès, and V. Aimez, "Extremely high aspect ratio GaAs and GaAs/AlGaAs nanowaveguides fabricated using chlorine ICP etching with N2-promoted passivation," Nanotechnology **21**(13), 134014 (2010).
31. H. Ishikawa and T. Kondo, "Birefringent phase matching in thin rectangular high-index-contrast waveguides," Appl. Phys. Express **2**, 042202 (2009).
32. S. J. B. Yoo, R. Bhat, C. Caneau, and M. A. Koza, "Quasi-phase-matched second-harmonic generation in AlGaAs waveguides with periodic domain inversion achieved by wafer-bonding," Appl. Phys. Lett. **66**(25), 3410–3412 (1995).
33. S. Gehrsitz, F. K. Reinhart, C. Gourgon, N. Herres, A. Vonlanthen, and H. Sigga, "The refractive index of AlxGa1-xAs below the band gap: Accurate determination and empirical modeling," J. Appl. Phys. **87**(11), 7825–7837 (2000).
34. S. Zollner, "Optical constants and critical-point parameters of GaAs from 0.73 to 6.60 eV," J. Appl. Phys. **90**(1), 515–517 (2001).
35. D. Duchesne, R. Morandotti, P. Cheben, B. Lamontagne, D.-X. Xu, S. Janz, and D. Christodoulides, "Group-index birefringence and loss measurements in silicon-on-insulator photonic wire waveguides," Opt. Eng. **46**(10), 104602 (2007).
36. A. Jaouad and V. Aimez, "Passivation of air-exposed AlGaAs using low frequency plasma-enhanced chemical vapor deposition of silicon nitride," Appl. Phys. Lett. **89**(9), 092125 (2006).

#146909 - $15.00 USD Received 3 May 2011; revised 4 Jun 2011; accepted 7 Jun 2011; published 10 Jun 2011

1. Introduction

Frequency conversion relying on quadratic electronic nonlinearities has sparked a vast amount of research focused on diverse applications including the generation of coherent sources in otherwise unattainable spectral regions [1], gas sensing [2], bio-photonics [3], time resolved spectroscopy [4], the realization of correlated photon pair sources [5], as well as all-optical signal processing for wavelength division multiplexing, routing and for solutions to wavelength contention [6]. In particular, nonlinear frequency mixing in waveguide devices offers several key breakthroughs, including compact on-chip integration and an important increase of the energetic efficiency when compared to traditional bulk crystals [6,7]. SHG is a second order nonlinear optical process, occurring in non-centrosymmetric materials, that converts two pump photons into a single photon at twice the pump frequency ($\omega + \omega \rightarrow 2\omega$) [8]. Efficient frequency conversion relies primarily on momentum conservation (phase matching) and the congruence between the spatial profiles of the input pump beam(s) and the generated harmonic. Due to the inherent material dispersion, momentum conservation is difficult to achieve, requiring the effective index at the fundamental wavelength to be equal to the effective index at the second harmonic for a type I interaction [$n_{eff}(\omega) = n_{eff}(2\omega)$]. This interaction has been nonetheless observed and exploited in numerous configurations using bulk media, and has been typically achieved through the use of birefringent crystals such as BBO and KTP [9], as well as in waveguide geometries [10–23] using polymers [10], $LiNbO_3$ [11], Ti-diffused $LiNbO_3$ [12], and semiconductors. In particular, SHG can be realized in isotropic GaAs, through either MPM [13–15], quasi-phase matching (QPM) [15–17], or artificially induced birefringence [15,18–20].

A surge of scientific activity has recently been devoted to developing novel phase matching techniques and to increasing the overall conversion efficiency in waveguiding structures [10–23], in an effort to develop a practical low power integrated frequency converter for all-optical signal processing systems and sensing/spectroscopy applications [1–7]. In particular, SHG was reported in AlGaAs/Al_xO_y with a record theoretical conversion efficiency of 20,000%/W/cm^2 (practical efficiency ~1400%/W/cm^2) [19], whereby phase matching and tight modal confinement were achieved through the introduction of thin Al_xO_y layers in the core of the waveguide, creating an artificial birefringence and thus removing the inherent isotropic nature of AlGaAs. On the other hand, quasi-phase matching, where the nonlinear tensor is periodically modulated with a period equal to twice the coherence length (either the material is poled, i.e. the orientation is patterned, for example by using regrowth techniques, or quantum-well intermixing is used; see [15,20,21] for an extensive list of QPM techniques) has also been reported in both $LiNbO_3$ [11] and GaAs [19], although the conversion efficiency is typically smaller than in birefringent matched schemes. SHG was also demonstrated in waveguides by exploiting modal birefringence between the first order fundamental frequency mode and the third order second harmonic mode [14, 15]. In these cases an 'M-shaped' waveguide has been utilized to enlarge the overall spatial modal overlap (resulting in an increased efficiency). Lastly, various exotic forms of phase matching have also been studied, including Bragg reflector waveguides [22], ring resonators [23], waveguide couplers [24], as well as embedded dichroic mirrors [19].

However, while many applications will benefit from these waveguide phase matching devices, inherent fabrication limitations prevent the practical and low-cost use of these structures in all-optical systems. In particular, artificial birefringence techniques require a complicated fabrication process in order to introduce (in the core of the waveguide) the selectively oxidized layers of Al required to achieve the necessary birefringence. QPM also necessitates complex fabrication procedures with periodic domain orientations, or quantum well intermixing. Similarly, M-shaped MPM waveguides require a costly two-step etching process. Integration of these devices on a single semiconductor chip with other components is practically unviable to date.

#146909 - $15.00 USD Received 3 May 2011; revised 4 Jun 2011; accepted 7 Jun 2011; published 10 Jun 2011

Here we exploit ultra-compact, simply structured AlGaAs photonic wires to simultaneously increase the overall SHG device efficiency through an increased overlap, and permit the large birefringence required to promote tunable phase matching across the telecommunication C-band. Using sub-mW CW input powers, we achieve MPM second harmonic generation via the interaction of the first order fundamental frequency mode at 1582nm with the third order second harmonic mode at 791nm, without the need of using an M-shaped waveguide. The theoretical maximum normalized efficiency for this device is 1110%/W/cm^2, comparable with the value reported for QPM and in other MPM devices [15]. On the other hand, we obtain a practical internal conversion efficiency of 13.8%/W/cm^2, limited mainly by losses. The potential success of this device is also related to the ease of fabrication, not requiring any complex oxidization or multi-etch steps of the waveguide material, while allowing for an adjustable phase matching condition (resulting in different phase matching wavelengths) which can be simply achieved by either tuning the temperature or the width of the waveguide (multiple width waveguides fabricated on the same chip). Moreover, the photonic wire structure proposed here can be used for several other operations, and has already been proven to be an ideal nonlinear platform for exploiting third order nonlinearities [25,26], for dispersion control [27] and for lowering the energetic requirements in all-optical switching [25,26], thus potentially allowing for ultracompact on-chip switching for all-optical telecommunications systems [28].

2. Device

The AlGaAs heterostructure proposed here was chosen due to the mature fabrication technology behind this platform, its broad infrared transparence, the ease of integrating devices with laser structures, as well as its inherently large second order nonlinear tensor, $\chi^{(2)}$ ~180pm/V, responsible for the overall strength of the SHG process [19,29]. The thicknesses and the aluminum concentrations of the various layers of the AlGaAs wafer (see Fig. 1b) were chosen to maximize the index contrast between the lower cladding and core, which is an essential requirement in tightly confined waveguides to prevent light leakage to the high-index substrate (i.e. GaAs). However, whereas choosing GaAs for the core and AlAs for the cladding material would serve as the highest index contrast pair, the bandgap of GaAs is ~870nm and would thus absorb any SH generated from a fundamental wave having a wavelength smaller than 1740nm. $Al_{20}Ga_{80}As$ was thus chosen as it allows for SHG with a fundamental wavelength within the 1500-1600nm spectral region. Furthermore, we avoided to use AlAs for the cladding, as it may (partially) oxidize and introduce further losses. The thickness of the core was set such that the fundamental mode (for widths of 400nm-800nm) is roughly circular in shape in order to maximize the spatial coupling with the experimentally available free space beam, and prevent light leakage to the substrate (in general, a tighter mode confinement requires a larger index contrast).

The fabrication of the waveguides was carried out by using plasma enhanced chemical vapor deposition to form a hard mask, followed by e-beam lithography for the definition of various waveguides widths *W*, ranging from 1000nm down to 300nm. Multiple inductively coupled plasma etching steps dedicated to each of the materials involved, such as the SiO_2 hard mask and the GaAs/AlGAs wafer, were then carried out to define high-contrast waveguides [30] with minimum propagation losses, as shown in Fig. 1a. The device was then cleaved to form 1.26mm-long ridge waveguides. The waveguide cross-section is presented in Fig. 1b, while Figs. 1c-e show the particular modes of the fundamental frequency (at the theoretically predicted phase matching wavelength of λ = 1582.32nm) and second harmonic (λ = 791.15nm) for a waveguide width of W = 650nm.

#146909 - $15.00 USD Received 3 May 2011; revised 4 Jun 2011; accepted 7 Jun 2011; published 10 Jun 2011

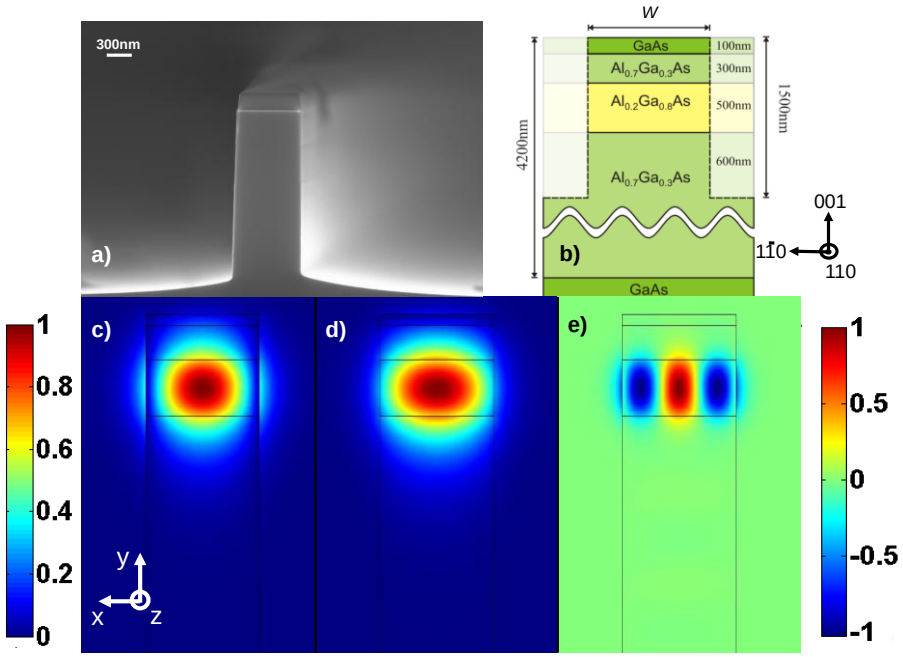

Fig. 1. (a) Scanning electron microscopy image of the fabricated waveguide device (width 650nm). (b) Corresponding heterostructure design, with widths W varying from 300nm to 1000nm. (c) Major electric field component of the horizontally (E_x) polarized fundamental mode at λ = 1582.32nm. (d) Major electric field component of the vertically (E_y) polarized fundamental mode at λ = 1582.32nm. (e) Major electric field component of the horizontally polarized (E_x) second harmonic mode at λ = 791.15nm.

3. Theory

As will be detailed below, the waveguides were written at 45 degrees relative to the crystallographic planes of the AlGaAs crystal (see Fig. 1 for the crystallographic plane alignment with respect to the waveguide coordinate system), thus forbidding a type I interaction with any of the modes presented in Figs. 1c-e. Instead, a specific case of type II evolution, where one pump photon of the x-polarized fundamental frequency combines with one photon from the y-polarized fundamental frequency to create an x-polarized photon at the second harmonic, was exploited in our case. The evolution equations governing this type of SHG are given by [8]:

$$\begin{aligned}
\partial_z E_{FF1} &= i\eta \exp(-i\Delta\beta z) E_{SH} E_{FF2}^* - \alpha_{FF1} E_{FF1}/2 \\
\partial_z E_{SH} &= i2\eta \exp(i\Delta\beta z) E_{FF1} E_{FF2} - \alpha_{SH} E_{SH}/2 \\
\partial_z E_{FF2} &= i\eta \exp(-i\Delta\beta z) E_{FF1}^* E_{SH} - \alpha_{FF2} E_{FF2}/2
\end{aligned} \tag{1}$$

where the effects of dispersion, group velocity mismatch and the time dependent nonlinear response of the nonlinearity have been dropped assuming a continuous wave excitation. The E_{FF1}, E_{FF2}, and E_{SH} are the electric field envelopes (in units of $W^{1/2}$) of the fundamental x-polarized beam, of the fundamental y-polarized beam, and of the second harmonic x-polarized beam, respectively (i.e. the electric field of the beam 'q' is given by $E = E_q F_q exp(i\beta_q z - i\omega_q t)$, where F_q is the transverse vectorial modal electric field distribution, β_q is the propagation constant, z is the longitudinal direction, ω_q is the angular frequency and t is the time coordinate). The phase mismatch factor is given by $\Delta\beta = \beta_{FF1} + \beta_{FF2} - \beta_{SH} = (n_{FF1} + n_{FF2} - 2n_{SH})\omega_{FF}/c$, where n_q refers to the effective refractive index of mode q at a given frequency.

#146909 - $15.00 USD Received 3 May 2011; revised 4 Jun 2011; accepted 7 Jun 2011; published 10 Jun 2011

The terms α_q are the linear loss coefficients for each mode q, and η is an overlap factor proportional to the normalized conversion efficiency (see below).

The basic principles related to SHG can be more intuitively understood by assuming a lossless and undepleted pump regime (power of the fundamentals P_{FF1}, P_{FF2} = constant). One can then readily solve the evolution equations to obtain the power of the SH signal:

$$P_{SH} = \eta^2 L^2 P_{FF}^2 \sin c^2 \left(\Delta\beta L / 2\right) \tag{2}$$

where L is the total length of propagation, P_{FF} is the total fundamental power equal to P_{FF1} + P_{FF2}. Furthermore, in arriving at Eq. (2), it was assumed that both the input pump beams have equal powers initially (P_{FF1} = P_{FF2}), which can be shown to give the maximum conversion efficiency [8]. Equation (2) explicitly relates the quadratic dependence of the generated second harmonic on the input power. One can also directly observe that the effects of phase matching are extremely important as the sinc squared function rapidly decays for $\Delta\beta L > 1.39$, allowing a narrow yet tolerable input bandwidth of ~0.6nm in our device. Moreover, we define the normalized conversion efficiency as:

$$\Gamma \equiv \frac{P_{SH}}{L^2 P_{FF}^2} \tag{3}$$

Note that Γ is measured in units of $W^{-1}m^{-2}$ but is typically reported as $100\cdot\Gamma$ (with corresponding units of $\%\cdot W^{-1}m^{-2}$). From Eq. (2) one obtains that the normalized conversion efficiency is $\Gamma = \eta^2$ for the case of perfect phase matching and in the absence of losses. Practically, losses are unavoidable and η^2 represents the theoretical maximum normalized conversion efficiency.

The evaluation of this term requires a vectorial analysis of the second order nonlinear interaction. In the crystallographic planes of the AlGaAs cubic crystal, the nonlinear tensor has a point group $\bar{4}3m$, of which all elements are zero except $\chi_{ijk}^{(2)} = \chi^{(2)}$ for $i \neq j \neq k$ [8]. However, whereas the heterostructure was grown along the 001 plane, our waveguides were electronically written parallel to 110 crystallographic direction (see Fig. 1b). In the basis of the waveguide axes, the nonlinear tensor must thus be rotated, and takes the new form in which the nonzero elements are as follows:

$$\chi_{xyx}^{(2)} = \chi_{xxy}^{(2)} = \chi_{yxx}^{(2)} = -\chi_{yzz}^{(2)} = -\chi_{zzy}^{(2)} = -\chi_{zyz}^{(2)} \equiv \chi^{(2)} \tag{4}$$

The overlap factor in this frame is thus given by [7, 31]:

$$\eta = \chi^{(2)} \sqrt{\frac{2\omega^2}{\varepsilon_0 c^3 n_{FF1} n_{FF2} n_{SH}}} \frac{\iint_{WG} G \cdot dxdy}{\sqrt{\iint |F_{FF1}|^2 dxdy} \sqrt{\iint |F_{FF2}|^2 dxdy} \sqrt{\iint |F_{SH}|^2 dxdy}}$$

$$\begin{aligned} G = {} & F_{FF1x} F_{FF2x} F_{SHy} + F_{FF1x} F_{FF2y} F_{SHx} + F_{FF1y} F_{FF2x} F_{SHx} \\ & - F_{FF1y} F_{FF2z}^* F_{SHz} - F_{FF1z}^* F_{FF2z}^* F_{SHy} - F_{FF1z}^* F_{FF2y} F_{SHz} \end{aligned} \tag{5}$$

where ε_0 is the permittivity of free space and the x,y,z subscripts indicate the vectorial components of the waveguide modes. While the overlap factor is given by 6 different overlap contributions, the dominant factor for the modes of interest (i.e. shown in Fig. 1c-e) is given by $F_{FF1x}F_{FF2y}F_{SHx}$, which represents all major components of the 3 implicated fields. Although it is not shown here, for the particular orientation of the waveguides in the AlGaAs crystallographic system analyzed here, a type I interaction is forbidden. The overlap factor for this interaction, given by Eq. (5), is zero due to the mixing of 2 symmetric and 1 antisymmetric components (involving the minor components of the fields) in the integral.

We also note that the square root of the normalized efficiency is inversely proportional to the area of the interaction:

#146909 - $15.00 USD Received 3 May 2011; revised 4 Jun 2011; accepted 7 Jun 2011; published 10 Jun 2011

$$\eta \propto \chi^{(2)} \sqrt{\frac{2\omega^2}{\varepsilon_0 c^3 n_{FF1} n_{FF2} n_{SH}}} \frac{1}{\Delta x \Delta y} \tag{6}$$

where the product $\Delta x \Delta y$ represents the modal field area of the interaction. It is thus extremely beneficial to reduce the waveguide core as much as possible to enhance the maximum normalized efficiency. However, it is important to realize that the overlap does reach a maximal value for a particular core size and further miniaturization leads to the modal fields losing their confinement (i.e. when a large part of the modal field resides in air where the $\chi^{(2)}$ is effectively 0) and thus a lower overlap [7,31].

4. Results and discussion

Using a wavelength-tunable CW laser, linearly polarized light at 45 degrees (to equally excite the two orthogonally-polarized fundamental modes) was coupled into the AlGaAs waveguide conversion device via standard end-fire coupling techniques using 50x (input and output) objective lenses. The output was sent to a Newport Oriel visible spectrometer for spectral measurements at the second harmonic wavelengths, whereas the absolute power scale of the spectrometer was calibrated using an Ophir PD-300uV power meter and a Thorlabs amplified photodetector PDA100A.

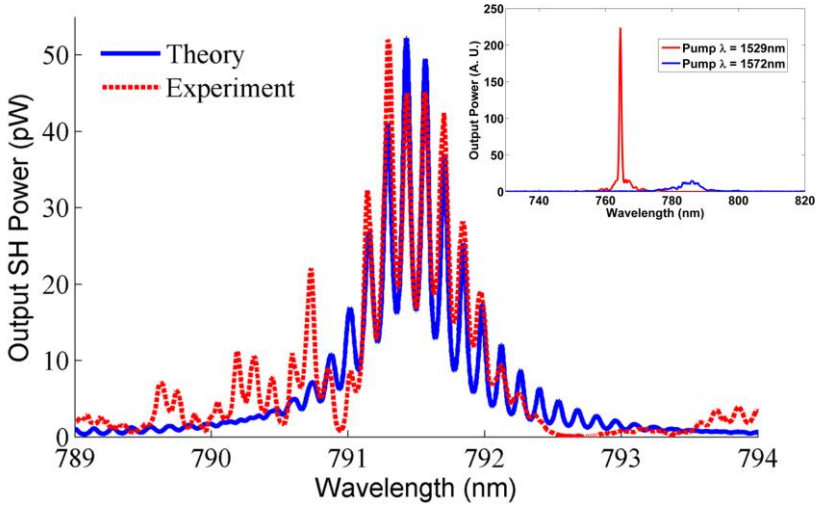

Fig. 2. Second harmonic signal power obtained in the 650nm-wide waveguide while scanning the CW input fundamental wavelength (experiment dashed red curve), showing a phase matching wavelength at 1582.6nm (791.3nm for the SH), and an allowable wavelength mismatch of ~1nm. The coupled input power was estimated to be 155μW. The high frequency fringes are a result of the fundamental wavelength Fabry-Perot effect. The blue solid curve is the theoretical fitting used to estimate the SH losses. Inset: Second harmonic signal power in the 600nm-wide waveguide when excited with a pulsed 100fs input laser source. An enhancement in the SH power is clearly observed at the phase matching wavelength of ~1529nm.

Phase matching was found experimentally for several different waveguide widths, the most efficient being in a 650nm-wide waveguide at a wavelength of 1582.6nm (with a second harmonic at 791.3nm). A low power, wavelength tunable, CW laser was used to characterize this device, and the results are presented in Fig. 2. It was determined that the maximum second harmonic signal was observed for an input polarization of 45 degrees, implying a type II interaction, whereas the output SH signal was horizontally (x-) polarized. The SHG signal power growth was also found to obey the expected quadratic relation as a function of the input CW power, as shown in Fig. 3. We estimated a normalized internal conversion

#146909 - $15.00 USD Received 3 May 2011; revised 4 Jun 2011; accepted 7 Jun 2011; published 10 Jun 2011

efficiency of 13.8%/W/cm^2, which is similar to previous results obtained using MPM in M-shaped waveguides [14] and in QPM in GaAs-based devices [15, 32]. A 100fs pulsed laser from an optical parametric oscillator was also used to compare the output second-harmonic power between the non-phase matched and phase matched SHG (see inset in Fig. 2). The latter measurements were performed in a waveguide with a width of W = 600nm in order to demonstrate a geometrical tunability of the phase matching condition.

In order to verify our findings, numerical simulations were performed using a vectorial finite-element method solver (Comsol Multiphysics). The material refractive indices were modeled according to [33], with modifications near the bandgap to account for absorption [34]. In the spectral region of interest, 1500nm–1600nm, the lowest order mode of the SH found to have phase matching with the first order mode of the fundamental frequency was the x-polarized third order mode depicted in Fig. 1e. The phase matching relation for this mode is shown in Fig. 4a (in addition to type I interactions that are forbidden in the considered geometry) for a waveguide width of 650nm. Moreover, the type II phase matching relation for these modes was studied for waveguides widths ranging from 450 to 1000nm (Fig. 4b). The simulated results agree extremely well with those obtained experimentally, with the phase matching wavelength at W = 650nm deviating by less than 0.5nm from the theoretically predicted value, and equally so for the 600nm-wide waveguide. Our simulations show that the phase matching wavelength can be easily tuned by simply using a different waveguide width. Moreover, the simulations also revealed the possibility to tune the phase matching wavelength by changing the temperature, with an approximate slope of 0.25nm/°C. Experimentally, we recorded a slightly larger shift of ~2nm for 3-4°C variations in temperature.

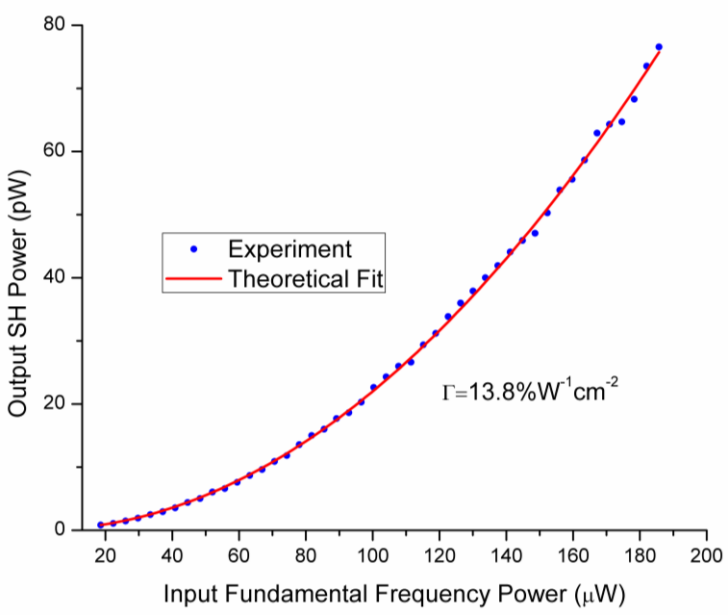

Fig. 3. Quadratic dependence of the generated second harmonic signal power on the fundamental frequency input CW power. An experimental normalized conversion efficiency of 13.8%/W/cm^2 is obtained.

The maximum normalized efficiency was numerically calculated to be 1110%/W/cm^2, which is roughly 80 times higher than the practical efficiency observed experimentally. This difference is attributed to the propagation losses of both the fundamental beams (measured to be 18.3dB/cm using the Fabry-Perot resonance technique [35]), and the second harmonic. To roughly estimate the SH losses, we solved Eqs. (1) including losses and the Fabry-Perot effect at the fundamental:

#146909 - $15.00 USD Received 3 May 2011; revised 4 Jun 2011; accepted 7 Jun 2011; published 10 Jun 2011

$$P_{SH} = \eta^2 L^2 P_{FF}^2 g / u_{FF1} u_{FF2}$$

$$g \equiv \frac{\exp(-\alpha_{SH} L)\left[\left(1-\exp(-\alpha L/2)\right)^2 + 4\exp(-\alpha L/2)\sin^2(\Delta\beta L/2)\right]}{(\Delta\beta L)^2 + (\alpha L/2)^2} \qquad (7)$$

$$u_i \equiv \left(1 - R_i \cdot \exp(-\alpha_i L)\right)^2 + 4R_i \cdot \exp(-\alpha_i L)\sin^2(\beta_i L)$$

where the function g represents the effects of losses and phase mismatch on the output second harmonic power (see a comparison to Eq. (2)). The Fabry-Perot formed by the waveguide end facets is represented by the oscillating functions u_i where R_i is the power reflectivity at the waveguide-air interface (note that the Fabry-Perot of the SH is negligible as $u_{SH} \approx 1$ due to the high losses) [35]. The theoretical SH tuning curve as a function of wavelength is presented in Fig. 2 (solid blue curve). The SH loss coefficient was extracted by fitting our theory to the experimental results, from which we obtained $\alpha_{SH} \approx 525$dB/cm. If we account for the presence of the tapers on the waveguide (which effectively prevents phase matching due to a different waveguide dispersion), the SH loss coefficient is reduced to 320 dB/cm. Very high losses at the second harmonic are typical (e.g. 250-350 dB/cm in [19]), and here are mainly attributed to the high field intensity of the SH mode (third order – see Fig. 1e) along the vertical waveguide walls, where scattering is particularly enhanced as a result of the residual roughness from the etching process. Numerically, we have estimated that any absorption of the SH in the top 100nm layer of GaAs (see Fig. 1b) is insignificant (<10dB/cm). Due to such losses, the optimal sample length is estimated to be ~4.75mm, after which the total converted SH power decreases rather than increases. For our sample length of 1.26cm, the experimental conversion efficiency amounts to 21.9%/W.

The previous discussion highlights the importance of reducing propagation losses for enhancing the experimental conversion efficiency. Recent passivation treatments have shown that it is possible to drastically reduce surface state absorption and scattering losses in these devices, thereby allowing future generation devices to achieve higher efficiencies [36]. From a design point of view, birefringent phase-matched structures, such as those reported by Fejer et al. [19], show a 20-fold increase in the theoretical normalized efficiency versus the structure analyzed here. This results from the higher modal overlap obtained by matching the first order modes at both the fundamental and the second harmonic frequencies. Nonetheless, our structure provides an appreciable efficiency while simultaneously not requiring complicated oxidation schemes, in turn providing a higher degree of integrability with other components, as well as lower fabrication costs.

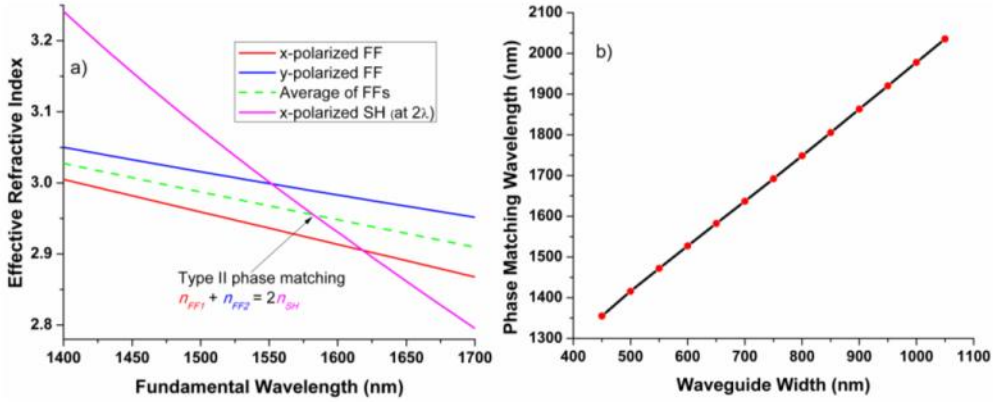

Fig. 4. Modal dispersion of the first order modes at the fundamental frequency and the third order mode at the second harmonic (plotted at twice the wavelength here) for a 650nm-wide photonic wire showing a phase matching wavelength at 1582.32nm for a type II interaction. (b) Theoretical phase matching wavelength vs waveguide width (for the same type II interaction).

#146909 - $15.00 USD Received 3 May 2011; revised 4 Jun 2011; accepted 7 Jun 2011; published 10 Jun 2011

5. Summary

In conclusion, we have experimentally demonstrated a highly compact AlGaAs frequency converter capable of operating with sub-mW CW powers. Modal phase matched SHG was shown using a waveguide having a core cross-section of 650nm x 500nm, and it was demonstrated that the phase matching wavelength of 1582.32nm could be tuned either by changing the waveguide width (i.e. by fabricating a chip with several waveguides of varying widths) or by tuning the temperature. The proposed photonic wire structure allows for a low-cost and mature fabrication technique not requiring selective oxidization, multiple etch steps of the waveguide material or complex wafer bonding strategies, while still obtaining a relatively high conversion efficiency. Our device holds much promise for future WDM applications, as a possible quantum correlated source using spontaneous parametric down conversion, and is the first step towards the demonstration of a totally integrated on-chip optical parametric oscillator.

Acknowledgements

This work was supported by the FQRNT (Le Fonds Québécois de la Recherche sur la Nature et les Technologies), the Natural Sciences and Engineering Research Council of Canada (NSERC), NSERC Strategic Projects, and the INRS. K. R. wishes to acknowledge a Marie Curie Outgoing International Fellowship (MOIF-CT-2006-039600).

#146909 - $15.00 USD Received 3 May 2011; revised 4 Jun 2011; accepted 7 Jun 2011; published 10 Jun 2011